14

A Parabolic Equation for Wave Propagation over Porous Structures

Tai-Wen Hsu and Jen-Yi Chang
Department of Hydraulic and Ocean Engineering, National Cheng Kung University, Tainan, Taiwan

1. Introduction

Porous structures such as seawalls, detached breakwaters, or submerged breakwaters are frequently used to protect shorelines from the effects of waves. The effectiveness of these structures is due to the fact that they are able to reflect, absorb, and dissipate wave energy. Wave energy reduction on the leeside of porous structures increases so that only a small part of the wave energy is transmitted to the nearshore. Consequently, the wave field on the leeside of such structures becomes quiet and the intensity of the wave action on the shoreline decreases; as a result, coastal erosion and the corresponding coastal disasters are mitigated. Wave transformation over porous structures must be understood in order to determine the stability of these porous structures and to evaluate their usefulness with regard to wave energy reduction.

Several numerical models have been developed to study the wave transformation over porous structures. Based on the mild-slope assumption, Rojanakamthorn et al. (1989) adopted Sollitt and Cross's (1972) theory to derive a modified mild-slope equation (MSE) for describing non-breaking waves traveling over a general finite porous bed. Later Rojanakamthorn et al. (1990) extended their model to the case of wave breaking on a submerged permeable breakwater. The validity of this model has been verified by comparing its numerical results with those of experiments and an analytical solution of a rectangular submerged breakwater.

The MSE is suitable for explaining the wave deformation of an unsteady flow in a porous structure that is linearized using an approximation of the nonlinear friction forces. The wave energy dissipation due to resistance in the porous structure is considered in the model and the depth-averaged equation yields an elliptic-type MSE on a permeable bed. Losada et al. (1996) presented the results of studies similar to that of Rojanakamthorn et al. (1990) for the kinematics and dynamics of wave interaction with permeable breakwaters that encounter non-breaking obliquely incident regular waves and directional random waves. The influence of structural geometry, properties of porous materials, and wave characteristics over and inside the breakwaters was also investigated. Following Rojanakamthorn et al. (1990) and Losada et al. (1996), Mèndez et al. (2001) derived a theory to analyze the influence of wave reflection and energy dissipation in wave breaking and porous flow, as induced by a porous submerged structure. The analytical expressions for the second-order

Source: Wave Propagation in Materials for Modern Applications, Book edited by: Andrey Petrin,
ISBN 978-953-7619-65-7, pp. 526, January 2010, INTECH, Croatia, downloaded from SCIYO.COM

mean quantities mass flux, energy flux, radiation stress, and mean water level are given in terms of the shape functions of the structure.

With increases in the number of available design possibilities, engineers want to work with increasingly larger coastal regions; however, it is still necessary for a simpler model to be applied in these situations—one that can provide reliable results to the practical questions posed. An evolution equation of mild slope equation (EEMSE) usually selected to simulate the combined wave refraction-diffraction in the vicinity of porous structures. The main reason for developing such a model is that it can predict coastal processes on a regional scale so that coastal changes resulting from driving forces and man-made structures can be determined. This wave information can be used as forcing functions to drive models that calculate alongshore and on-offshore sediment transports. Numerical wave models such as RCPWAVE (Ebersole et al., 1986), REF/DIF-1 (Kirby and Dalrymple, 1991), and the Parabolic Wave Model (Mordane et al., 2004), all of which neglect the wave reflection, are frequently used as tool for predicting coastal erosion and deposition.

The main purpose of this paper is to extend the EEMSE addressed by Hsu and Wen (2001) and Hsu et al. (2008b) for waves propagating over submerged permeable structures in the surf zone. The governing equation is a parabolic formulation of the EEMSE including the breaking and energy dissipation effect of porous structures. The approximate MSE enables a more accurate description of combined wave refraction, diffraction and reflection in the computational domain. Following Rojanakamthorn et al. (1990), wave breaking and energy dissipation of porous structures are accounted for in a relatively straightforward manner by adding an energy dissipation coefficient to the EEMSE. An implicit finite-difference approximation scheme is implemented in the numerical solution. Several numerical cases were computed and compared through experiments to examine the validity of the present model. This model was also applied to practical cases of wave-height evolution in the vicinity of the submerged permeable structures over a complicated bathymetry.

2. Theoretical formulation

2.1 Governing equation

The definition sketch for linear periodic waves propagating over a submerged permeable structure in the surf zone is shown in Fig. 1, where h is the local water depth of the pure water region and h_p, the thickness of the porous layer. Following Rojanakamthorn et al. (1989), the MSE for describing the wave deformation over porous structures is derived by multiplying the Laplace equation using corresponding vertical eigenfunctions solved by Sollitt and Cross (1972). In this paper, wave breaking, energy dissipation, and large-angle incidence are included in the MSE. Based on Rojanakamthorn et al. (1989), the MSE is formulated to consider the wave transformation over porous structures, as given by

$$\nabla_h \cdot \left(\alpha_p \nabla_h \phi \right) + k_0^2 \alpha_p \left(1 + i f_d \right) \phi = 0 \tag{1}$$

where $\phi(x,y)$ is the complex velocity potential; $\nabla_h = (\partial/\partial x, \partial/\partial y)$, is the horizontal gradient operator; k_0, is the complex wavenumber; f_d, is the energy dissipation factor in the surf zone after wave- breaking; and α_p, is a parameter expressed by

$$\alpha_p = \alpha_1 + n_0 \left(S - i f_p \right) \alpha_2 \tag{2}$$

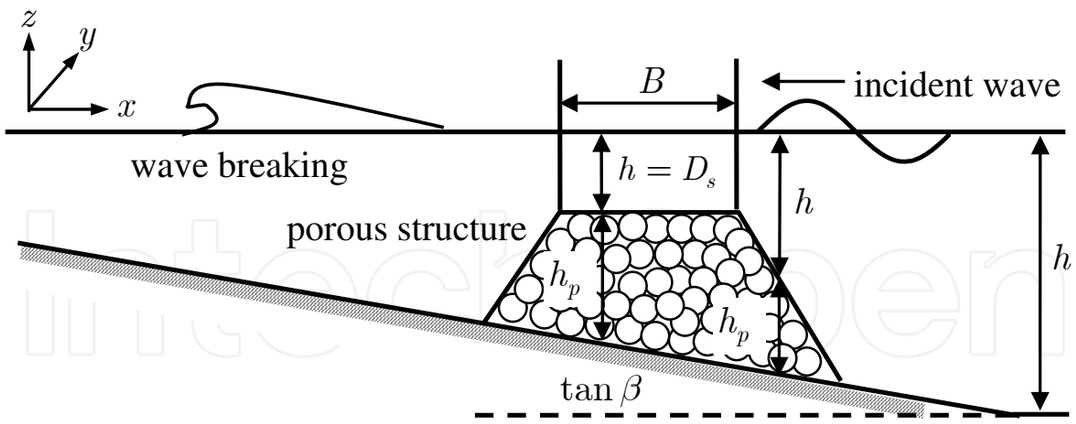

Fig. 1. Waves propagating over a submerged permeable structure.

where α_1 and α_2 are respectively given by

$$\alpha_1 = h\beta_1^2\left[\frac{\beta_2^2\left(1-e^{-2k_0h}\right)}{2k_0h} - \frac{\beta_3^2\left(1-e^{2k_0h}\right)}{2k_0h} - 2\beta_2\beta_3\right] \tag{3}$$

$$\alpha_2 = \frac{1}{2}h\beta_1^2\left[1+\frac{\sinh\left(2k_0h_p\right)}{2k_0h_p}\right] \tag{4}$$

$$\beta_1 = \frac{1}{n_0e^{k_0h}\sinh\left(k_0h_p\right)-\delta_p\cosh\left(k_0h\right)} \tag{5}$$

$$\beta_2 = n_0e^{k_0h}\sinh\left(k_0h_p\right)-\frac{1}{2}\delta_pe^{k_0h} \tag{6}$$

$$\beta_3 = \frac{1}{2}\delta_pe^{-k_0h} \tag{7}$$

$$\delta_p = n_0\sinh\left(k_0h_p\right)-\left(S-if_p\right)\cosh\left(k_0h_p\right) \tag{8}$$

in which n_0 is the porosity of the permeable material; $S = n_0 + (1-n_0)C_M$, the inertial coefficient; C_M, the virtual mass coefficient; f_p, a linear friction coefficient; and $i = \sqrt{-1}$, a unit complex number. Following Radder (1979), a scale factor

$$\varphi = \sqrt{\alpha_p}\phi \tag{9}$$

is introduced into Eq. (1) and the mathematical manipulation yields the Helmholtz equation

$$\nabla_h^2\varphi + k_c^2\varphi = 0 \tag{10}$$

where k_c is a pseudo-wavenumber written in the form

$$k_c^2 = k_0^2\left(1+if_d\right) - \frac{\nabla_h^2\sqrt{\alpha_p}}{\sqrt{\alpha_p}} \tag{11}$$

The complex wavenumber can be determined through the following dispersion relation:

$$\omega^2 = gk_0\frac{n_0e^{k0h}\sinh\left(k_0h_p\right)-\delta_p\sinh\left(k_0h\right)}{n_0e^{k0h}\sinh\left(k_0h_p\right)-\delta_p\cosh\left(k_0h\right)} \tag{12}$$

where ω is the angular frequency and g, the gravitational acceleration. The wave motion is assumed to be purely harmonic in time. Equation (10) is easily split into two equations by using the commuting operators $\partial/\partial x$ and $\left(1/k_c^2\right)\partial^2/\partial^2 y$:

$$\left(\frac{\partial}{\partial x}-ik_c\sqrt{1+X}\right)\left(\frac{\partial}{\partial x}+ik_c\sqrt{1+X}\right)\phi = 0 \tag{13}$$

where X is the orthogonal operator given by

$$X = \frac{1}{k_c^2}\frac{\partial^2}{\partial y^2} \tag{14}$$

In Eq. (13), it is noted that the wave field is split into forward- and backward-scattering fields. As mentioned, solving the MSE incurs a significant computational cost whenever large coastal areas are considered. In these circumstances, a simpler method can provide an efficient and reliable tool to solve practical problems. The combined effect of wave refraction and diffraction in the vicinity of shoals, islands, and coastal structures can be simulated by a parabolic approximation in which the wave reflection is neglected. Although the wave reflection might be important for submerged structures, it is usually ignored in the model for solving practical coastal engineering problems such as nearshore current, sediment transport, and ocean environment pollution. The inference of reflection will be considered in section 6.

Eq. (13) is thus simplified as

$$\left(\frac{\partial}{\partial x}-ik_c\sqrt{1+X}\right)\phi = 0 \tag{15}$$

According to Sollitt and Cross (1972), the linear friction factor f_p is evaluated from Lorentz's condition of equivalent work, and this relation can be expressed as

$$f_p = \frac{1}{\omega}\frac{\int_\forall\int_0^T\left(\frac{n_0^2\upsilon}{k_p}\left|\vec{u}_s\right|^2+\frac{n_0^3C_p}{\sqrt{k_p}}\left|\vec{u}_s\right|^3\right)dtd\forall}{\int_\forall\int_0^T n_0\left|\vec{u}_s\right|^2\,dtd\forall} \tag{16}$$

where $\forall$ is the volume of the flow field; T the wave period; υ the kinematic viscosity; k_p the intrinsic permeability; C_p the turbulent friction coefficient; and $\vec{u}_s = -\nabla_h \phi$ the seepage velocity vector. The value of f_p is obtained through an iterative technique suggested by Sollitt and Cross (1972). The detailed procedure will be briefly presented in the following section. The values of k_p and C_p are usually determined through laboratory tests; however, it is difficult to estimate their proper values in practical applications without experiments. Some empirical formulae may be applicable in the computation. Following Furukawa and McDougal (1991), the value of the intrinsic permeability k_p is determined by the empirical formula:

$$k_p = 1.643 \times 10^{-7} \left(\frac{d_{50}}{10} \right)^{1.57} \frac{n_0^3}{(1-n_0)^2} \tag{17}$$

where d_{50} is the grain or gravel diameter in millimeters. If the porous materials are stones or armor units, it is plausible that one could calculate the diameter using the equivalent volume of the sphere. The coefficient C_p that describes the resistance properties of porous media is generally estimated from experiments under steady flow conditions. Arbhabhiramar and Dinoy (1973) conducted laboratory tests and proposed a formula through experimental data:

$$C_p = 3.162 \times 10^6 \left[d_{50} \sqrt{\frac{n_0}{k_p}} \right]^{-1.50} \tag{18}$$

It is noted that Eqs. (11) and (12) are reduced to the expressions of the pseudo-wavenumber $k_c^2 = k_0^2 - \nabla_h^2 \sqrt{CC_g} \Big/ \sqrt{CC_g}$ and the dispersion relation $\omega^2 = g k_0 \tanh k_0 h$ for the case of impermeable structures without wave breaking and energy dissipation, respectively. These results are identical to those of Mordane et al.'s (2004) theoretical formulations.

2.2 Wave energy dissipation

In order to describe the wave breaking and energy dissipation of waves propagating over a porous structure, many empirical formulae can be used in the MSE. For energy dissipation after wave breaking over an impermeable bed, Dally et al. (1985) used the hydraulic jump model to account for the energy dissipation. Battjes and Janssen (1978) estimated the energy dissipation by means of periodic bores. Isobe (1987) adopted a turbulence model to represent the energy losses of breaking waves; this model was later modified by Watanabe and Dibajnia (1988) from comparisons of model calculations and experimental data. In order to define the region of the surf zone, many criteria have been utilized to determine the breaking point; these include criteria based on theoretical formulations and empirical relationships such as those of Miche (1951), Goda (1970), and Isobe (1987) and others.

It is desirable to find a more suitably coupled formula for describing the wave breaking and energy dissipation for porous structures in MSE. When studying the possible combinations of these empirical formulae, experimental data from permeable beds are rare. Rojanakamthorn et al. (1990) adopted Watanabe and Dibajnia's (1988) model to derive a new equation for describing the processes of wave decay and recovery due to porosity and wave breaking; therein, a similar mechanism of energy loss between impermeable and

permeable beds is assumed. Based on their equation, the energy dissipation formulae mentioned above are selected to account for wave deformation on the porous structures across the surf zone. The energy dissipation coefficients related to wave breaking and porosity are finally expressed as

$$f_d = \frac{k_r}{C_g}\frac{K_2}{k_r h'}\left(1-\frac{K_1^2}{\gamma^2}\right) \tag{19a}$$

$$f_d = \frac{k_r}{C_g}\frac{\alpha' Q_b}{n\pi}\left(\frac{H_{\max}}{H_{rms}}\right)^2 \tag{19b}$$

$$f_d = \frac{k_r}{C_g}\alpha_D \tan\beta\sqrt{\frac{g}{h'}}\sqrt{\frac{\gamma-\gamma_r}{\gamma_s-\gamma_r}} \tag{19c}$$

where K_1, K_2, α', and α_D are calibrated parameters; k_r the real part of the progressive complex wavenumber k_0; $\gamma = H/h'$ the ratio of wave height to the effective water depth h'; $\gamma_r = 0.4\left(H/h'\right)_b$ the critical value of a recovery wave on h' ; $\gamma_s = 0.8\left(0.57+5.3\tan\beta\right)$ a ratio of wave height to h'; $H_{\max} = \left(0.88/k_r\right)\tanh\left(\gamma_0 kh/0.88\right)$ the maximum wave height; H_{rms} = the root mean square value of wave height; $Q_b = \exp\left[\left(1-Q_b\right)/\left(H_{rms}/H_{\max}\right)^2\right]$; $\gamma_0 = 0.5+0.4\tanh\left(33H_0/L_0\right)$; and $\tan\beta$ the average bottom slope calculated from the breaking point to an offshore distance $5h_b'$. The subscript "b" denotes the value at the breaking point. For regular waves, the value of Q_b equals 1 and H_{rms} is replaced by H_0. Based on Losada et al. (1997), the effective water depth h' is used to be instead of h in the energy dissipation model in order to consider the porosity of the structure which is given by

$$h' = \frac{1}{k_r}\tanh^{-1}\left(\frac{\omega^2}{gk_r}\right) \tag{20}$$

A breaking index is used as a criterion to define the incipient breaking point of breaking waves traveling over a permeable structure. The following breaking criteria of an impermeable bed as presented by Miche (1951), Goda (1970), and Isobe (1987), respectively are modified in the wave calculations for porous structures:

$$\gamma_b = 0.142\frac{L_b}{h_b'}\tanh\frac{2\pi h_b'}{L_b} \tag{21a}$$

$$\gamma_b = 0.17\left\{1-\exp\left[-1.5\frac{\pi h_b'}{L_0}\left(1+15\left(\tan\beta\right)^{4/3}\right)\right]\right\} \tag{21b}$$

$$\gamma_b = 1.06-0.6\exp\left(-3\sqrt{h_b'/L_0}\right)+10\left(\tan\beta\right)^{3/2}\cdot\exp\left[-45\left(\sqrt{h_b'/L_0}-0.1\right)^2\right] \tag{21c}$$

where γ_b is the wave breaking index defined by $\gamma_b = H_b/L_b$ and H_b and L_b, are the breaking wave height and wavelength, respectively. Eqs. (19) and (21) are respectively

selected to form a coupled equation to solve the energy dissipation due to porosity and wave breaking.

In practical applications, the parameters α_D, K_1, K_2, and γ' are determined experimentally. According to the analysis of Mèndez et al. (2001), $\alpha_D = 1.0$, $K_1 = 0.4$, $K_2 = 0.35$, and $\alpha' = 1.0$ were suggested in the numerical simulation. Nine sets of coupled equations were examined in the computation. In order to find a more suitable coupled equation for solving the wave breaking and energy dissipation on a porous structure, two sets of experimental data (Cruz et al. 1997; Lara et al. 2006) were used by Hsu et al. (2008a) to examine the applicability of the nine coupled equations. A comparison of the model results and experimental data is presented in Table 1. It is observed that the combination of Eqs. (19c) and (21b) achieves the best agreement with observations in which a higher correlation coefficient C_R is obtained, where C_R is defined by

$$C_R = 1 - \sqrt{\frac{1}{N}\sum_{i=1}^{N}\frac{\left[(H_m)_i - (H_c)_i\right]^2}{\left[(H_m)_i\right]^2}} \tag{22}$$

where N is the total number of observed data points; H_m the value measured from laboratory experiments; and H_c the value calculated from the model. As a result, this coupled equation is used in the study to calculate wave breaking and energy dissipation on permeable structures.

Eq.(19) \ Eq.(21)	Miche(1951) (Eq.(21a))	Goda(1970) (Eq.(21b))	Isobe(1987) (Eq.(21c))
Dally et al.(1985) (Eq.(19a))	0.845	0.831	0.853
Battjes and Janssen (1978) (Eq.(19b))	0.799	0.818	0.788
Watanabe and Dibajnia (1988) (Eq.(19c))	0.859	0.871	0.846

Table 1. Comparisons of the correlation coefficients C_R using different coupled equations of breaking criteria and energy dissipation formulae.

2.3 Parabolic approximations

In Eq. (15), it should be noted that different approximations of the function $\sqrt{1+X}$ will lead to different orders of the parabolic equations. The most classical approximation is an expansion of the Taylor series, wherein a series with a greater number of terms could lead to a better approximation of the incident wave angle. However, this is a time-consuming process due to the large matrix dimension inherent in a large coastal environment; this would results in a disadvantage of the numerical calculation. An alternative to the rational function approximation permits us to improve the angular capacity of the incident angle as well as the computational effort by summing a relatively fewer number of terms related to the Taylor series. In this investigation, following Mordane et al. (2004), we selected a quadratic rational function of the Padé [2,2] approximation, given by

$$\sqrt{1+X} = \frac{P_0 + P_1 X + P_2 X^2}{Q_0 + Q_1 X + Q_2 X^2} + O\left(X^5\right) \tag{23}$$

where P_i and Q_i $(i=0,1,2)$ are Padé coefficients. Several methods can be used to obtain the Padé coefficients. According to St. Mary (1985), these coefficients are determined using an ad-hoc technique of Chebychev referred to as Pkni = { $P_0 = 1.628909$, $P_1 = 2.428289$, $P_2 = 0.8308198$, $Q_0 = 1$, $Q_1 = 1.615038$, $Q_2 = 0.235499$ }. In the present model, Pkni is used to model a wave traveling in very large coastal areas of several wavelengths. Mordane et al. (2004) showed that the maximal propagation wave angle of Pkni coefficients is around 77°. Substituting Eq. (23) into Eq. (15) yields the following expression:

$$\left(Q_0 + Q_1 X + Q_2 X^2\right)\frac{\partial \varphi}{\partial x} = ik_c\left(P_0 + P_1 X + P_2 X^2\right)\varphi \tag{24}$$

Eq. (24) can be further derived using the expressions $X = \left(1/k_c^2\right)\partial^2/\partial^2 y$ and $X^2 = \left[\left(1/k_c^2\right)\partial^2/\partial^2 y\right]^2$; the resulting equation is

$$\left(\lambda_1 + \lambda_2\frac{\partial^2}{\partial y^2} + \lambda_3\frac{\partial^3}{\partial y^3} + \lambda_4\frac{\partial^4}{\partial y^4}\right)\frac{\partial \varphi}{\partial x} = ik_c\left(\vartheta_1 + \vartheta_2\frac{\partial^2}{\partial y^2} + \vartheta_3\frac{\partial^3}{\partial y^3} + \vartheta_4\frac{\partial^4}{\partial y^4}\right)\varphi \tag{25}$$

where the corresponding coefficients are given by $\lambda_1 = Q_0$, $\lambda_2 = \left(Q_1/k_c^2\right)$ $+\left(2Q_2/k_c^5\right)\left[\left(3/k_c\right)\left(\partial k_c/\partial y\right)^2 - \left(\partial^2 k_c/\partial y^2\right)\right]$, $\lambda_3 = -\left(4Q_2/k_c^5\right)\left(\partial k_c/\partial y\right)$, $\lambda_4 = Q_2/k_c^4$, $\vartheta_1 = P_0$, $\vartheta_2 = \left(P_1/k_c^2\right) + \left(2P_2/k_c^5\right)\left[\left(3/k_c\right)\left(\partial k_c/\partial y\right)^2 - \left(\partial^2 k_c/\partial y^2\right)\right]$, $\vartheta_3 = -\left(4P_2/k_c^5\right)\left(\partial k_c/\partial y\right)$ and $\vartheta_4 = P_2/k_c^4$. Equation (25) is a fifth-order partial differential equation, and it can be applied to simulate wave transformation over porous structures, including wave breaking and energy dissipation. We notice that the finite difference equations can be obtained by making the governing equation discrete; they are solved by a standard Crank-Nicholson scheme for traditional partial differential equations. The details of the numerical scheme are provided in the paper of Mordane et al. (2004).

It follows that by differentiating the Helmholtz equation with respect to y and using the rigid boundary condition, the boundary conditions of Eq. (25) are thus given by

$$\frac{\partial \phi}{\partial y}(x, y_0) = 0,\ \frac{\partial \phi}{\partial y}(x, y_m) = 0 \tag{26}$$

$$\frac{\partial^3 \phi}{\partial y^3}(x, y_0) = 0,\ \frac{\partial^3 \phi}{\partial y^3}(x, y_m) = 0 \tag{27}$$

for all x, where y_0 and y_m are the initial and terminal points of the lateral boundary, respectively. By using a central finite difference to discretize the boundary conditions of Eqs. (26) and (27) and by introducing the fictitious points $\varphi_{i,-1}$, $\varphi_{i,-2}$, $\varphi_{i,m+1}$, and $\varphi_{i,m+2}$, the boundary conditions in this model can be reduced to $\phi_{i,-1} = \phi_{i,1}$, $\phi_{i,m+1} = \phi_{i,m-1}$, $\phi_{i,-2} = \phi_{i,2}$, and $\phi_{i,m+2} = \phi_{i,m-2}$.

For a large wave angle incidence, the radiation boundary condition is also specified by Eq. (15) and approximated by Eq. (25). However, it is too complicated to achieve the matrix

formulation by using Eq. (25) as the boundary conditions in the numerical solution. An alternative method is to rotate the computational domain, in order to ensure that the given boundary is always normal to the incident wave direction. This method enables us to change the radiation boundary conditions as the rigid boundary conditions at the lateral boundary.

3. Model verifications

The applicability and validity of the present model were verified through experiments in which waves propagated over impermeable composite uniform slope, submerged permeable breakwaters and sloping beaches. In the first case, Nagayama (1983) measured wave deformation on a bar-type beach profile. It consists of three sections of slope 1/20 and the wave deformation includes shoaling, first breaking, wave decay, wave recovery and the of second breaking. The experimental conditions are $H_0 = 0.07$ m and $T = 0.94$ s, respectively. Fig. 2. shows the comparison of wave height between the numerical simulation of the present model and experimental data. It can be seen from the figure that the numerical results follow the experimental data fairly well.

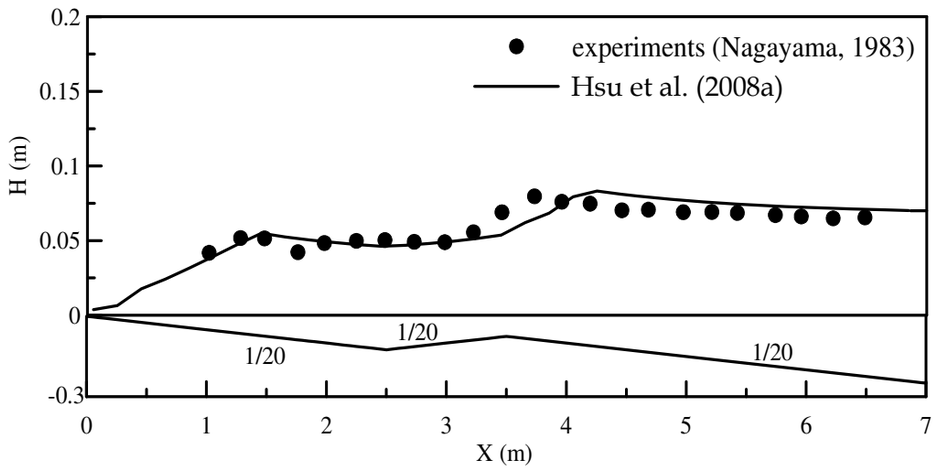

Fig. 2. Comparison of calculated wave height and experimental results for waves passing over a composite slope.

The experimental data were obtained from Rojanakamthorn et al. (1989) for a wave flume with a length, width, and depth of 23 m, 0.8 m, and 1 m, respectively. The breakwater comprises gravel with an average diameter of 26 mm that was placed on an impermeable and uniform slope of 1/20, approximately 2 m from the toe of the slope. The front slope of the breakwater is approximately 1/3. The experimental conditions are summarized in Table 2, where H_0 is the incident wave height; D_s, the water depth above the structure; and B, the width of the structure (Fig. 1).

According to Hsu et al. (2008a) the key parameters $n_0 = 0.39$, $k_p = 3.77 \times 10^{-7}$ m^2, and $C_p = 0.332$ were used in the computation; these are identical to those used by Rojanakamthorn et al. (1989). The added mass coefficient arose due to the unsteady convergence and divergence of streamlines around a solid body. Since the unsteady flow around a body with a complicated shape has not been fully clarified, the coefficient C_M is

not readily determined for randomly and densely packed solid materials. Therefore, based on to Sollitt and Cross (1972) and Madsen (1974), the inertial coefficient S is approximately regarded as unity for this computation.

The numerical calculation in the Hsu et al.'s (2008a) model includes an iteration procedure for f_p. Following Rojanakamthorn et al. (1989) and for convenience, the initial value of f_p is first estimated as unity. For a given incident wave condition, the local complex wavenumber k_0 is estimated from Eq. (12) through the iteration technique. The coefficient α_p is next computed from Eqs. (2) to (8); the scale factor φ and the seepage velocity vector $\vec{u}_s$ are then determined at every grid point. The value of f_p is again estimated from Eq. (16). The iteration procedure is repeated until the change in f_p is less than a tolerance of the relative error $\varepsilon = 10^{-2}$. Details of the numerical scheme are referred to Hsu et al. (2008a).

A comparison of the model results with those of the laboratory experiments is shown in Fig. 3; these results are found to be in good agreement. It is observed from Fig. 3 that the wave amplitude rapidly decreases while waves propagate over the submerged permeable breakwater due to energy decay on the porous structures. We note that in the free surface of the experiments, the model results were unable to catch the modulations. On the other hand, the values of f_p are different from those given in Rojanakamthorn et al. (1989) (see Table 2). The difference in values may be caused by neglecting certain physical processes such as wave reflection or different numerical schemes (parabolic or elliptic type of MSE) in the model.

Items / Authors	slopes	H_0 (m)	d_{50} (mm)	T (sec)	h (m)	B (cm)	D_s (cm)	n_0	k_p (m^2)	C_p	f_p
Rojanakamthorn et al. (1989)	1/20	0.0471	20-35	0.93	0.375	10	6.5	0.39	3.77E-7	0.332	(1.155)0.412
	1/20	0.0321	20-35	0.93	0.375	30	6.5	0.39	3.77E-7	0.332	(1.039)0.384
	1/20	0.0472	20-35	1.08	0.375	235	8.0	0.39	3.77E-7	0.332	(1.507)0.871
Cruz et al. (1997)	1/20*; 1/6.67+	0.0220	6.7	1.02	0.176	—	—	0.44	2.5E-8	0.40	(2.576)
	1/20*; 1/6.67+	0.0430	6.7	1.00	0.1748	—	—	0.44	2.5E-8	0.40	(2.557)
Lara et al. (2006)	1/20	0.15	—	2.0	0.4	—	—	—	—	—	—
	1/20	0.15	19	2.0	0.4	—	—	0.49	(2.036E-7)	(0.624)	(5.726)
	1/20	0.15	39	2.0	0.4	—	—	0.49	(6.296E-7)	(0.495)	(2.495)
	1/20	0.15	—	3.0	0.4	—	—	—	—	—	—
	1/20	0.15	19	3.0	0.4	—	—	0.49	(2.036E-7)	(0.624)	(6.520)
	1/20	0.15	39	3.0	0.4	—	—	0.49	(6.296E-7)	(0.495)	(1.829)

Table 2. Experimental conditions for wave propagating over submerged permeable breakwaters (* : the front slope; + : the rear slope. Values in brackets were calculated by the present model.)

The model is also applied to simulate wave transformation on a porous sloping bottom. Experiments were performed by Cruz et al. (1997) in a 0.30 × 0.20 × 11.0 m wave flume at the University of Tokyo, Japan. The bathymetry of the sloping bottom is shown in Fig 3. The triangular porous bar side slopes of are 1:20 and 1:6.67, respectively. The key parameters $n_0 = 0.44$, $k_p = 2.5 \times 10^{-8}\,\mathrm{m}^2$, and $C_p = 0.4$ were used in the computation, as suggested by Cruz et al. (1997). The experimental conditions are listed in Table 2. A comparison of the

numerical results and experiments for the two cases (Table 2) is shown in Fig. 4. Fig 4(a) shows the measured and computed wave heights for an incident wave with small damping without breaking. It is evident that the general trend of the damped wave height is approximated quite well by the model. In Fig 4(b), the propagating wave breaks at around $x = 5.8$ m. The computed and observed wave heights are in good agreement.

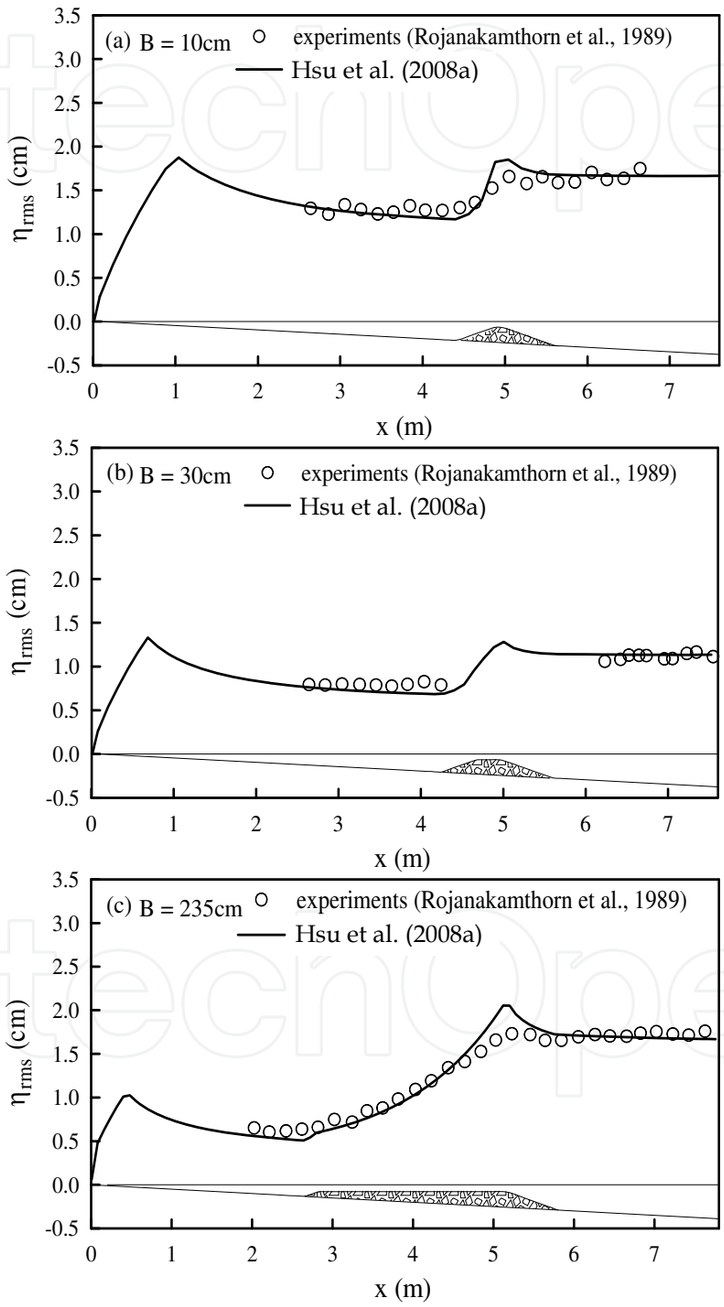

Fig. 3. Distribution of root mean square value of water surface elevations. (a) $B = 10$ cm; (b) $B = 30$ cm; and (c) $B = 235$ cm.

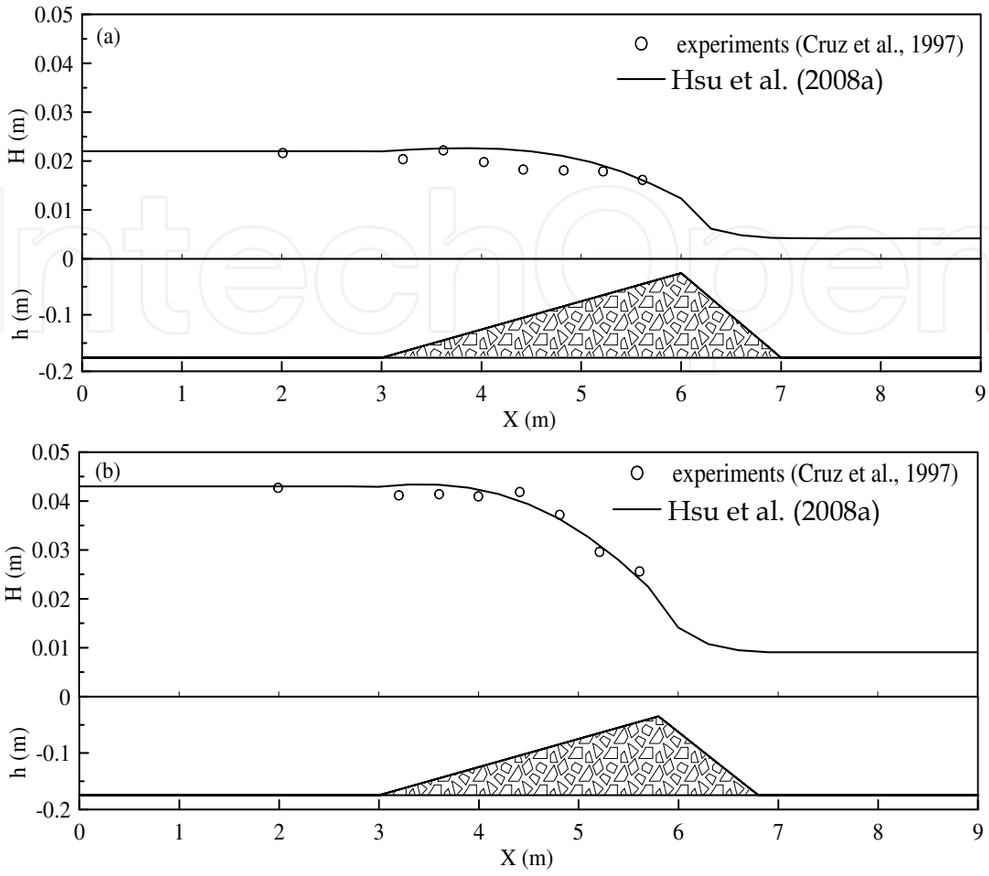

Fig. 4. Wave transformation on plane porous slope. (a) H_0 = 0.022 m; T = 1.02 s and (b) H_0 = 0.043 m, T = 1.00 s.

Numerical simulations of the wave breaking processes over a gravel sloping bottom were also performed by Hsu et al. (2008a) and compared with the experimental data provided by Lara et al. (2006). Experiments were conducted in a wave flume with a length, width, and depth of 24 m, 0.6 m, and 0.8 m, respectively. Two sloping layers with a porosity of $n_0 = 0.49$ were constructed with different mean gravel diameters— $d_{50} = 19$ mm and 30 mm, respectively. These key parameters were used to estimate the values of k_p and C_p by Eqs. (17) and (18); f_p is obtained through an iteration procedure. Two different incident wave conditions $H_0 = 0.15$ m, $T = 2.0$ s and $H_0 = 0.15$ m, $T = 3.0$ s (Table 2) were selected to verify the capability of the present model. The types of wave breaking in these two cases are spilling breaker ($T = 2.0$ s) and plunging breaker ($T = 3.0$ s), respectively. The experimental conditions are summarized in Table 2. Fig. 5 shows the spatial variations of the wave heights from a shoaling zone to the still water level. The numerical results of Hsu et al. (2008a) model can reproduce the wave transformation over a permeable sloping bottom. Notably, under incident wave conditions, the breaking wave height, location of the breaking point, and wave decay caused by energy dissipation against breaking and porous gravel slopes were accurately predicted.

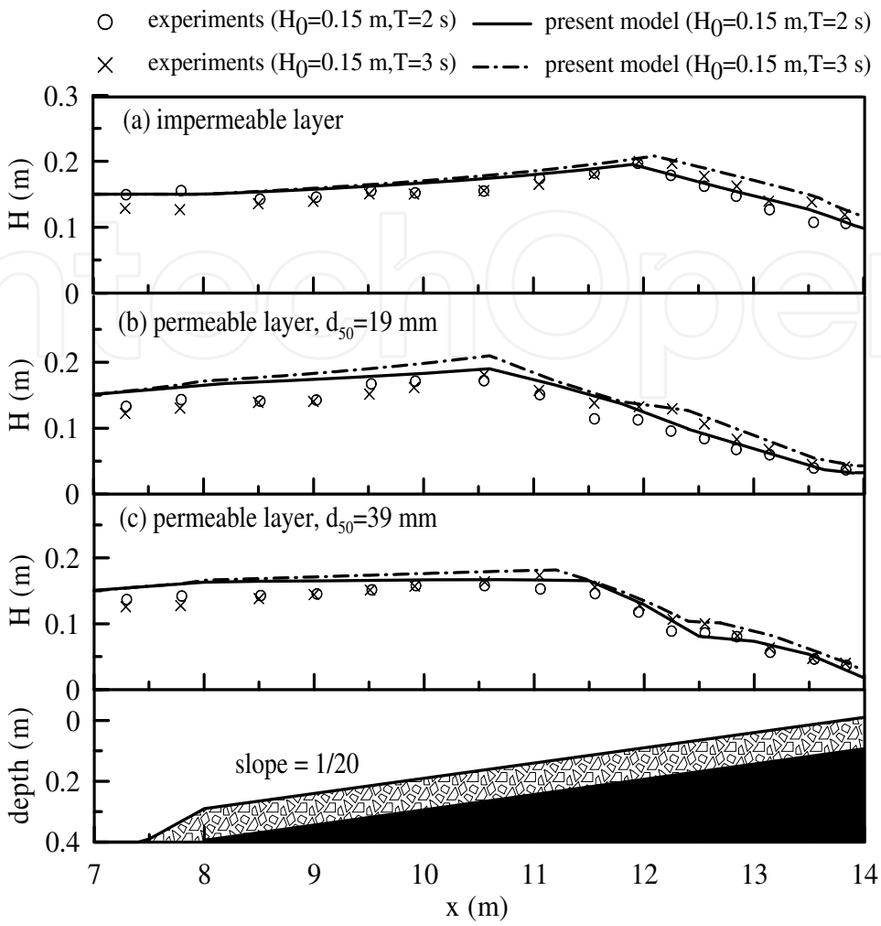

Fig. 5. Wave height evolution on permeable gravel slopes predicted by Hsu et al.'s (2008a) model. (a) impermeable layer; (b) permeable layer (d_{50} =19 mm); and (c) permeable layer (d_{50} =39 mm). The thickness of the porous layer is 11 cm. The experiments were carried out by Lara et al. (2006).

4. Experimental verification

In order to examine the validity of the present model, a large-scale experiment was conducted by Hsu et al. (2008a) in a three-dimensional wave basin to create waves propagating over a permeable submerged circular pile that is rested on a gravel sloping bottom with normal incidence. This model test was carried out in a laboratory of the National Cheng Kung University, Taiwan. As show in Fig. 6, the wave basin has a length, width, and depth of 40 m, 40 m, and 1.2 m. Waves were generated by two piston-type wavemakers, and a wave absorption system was installed on all the boundaries. The sloping bottom was carefully constructed in concrete with straight and parallel contours that made an angle of 15° with the wave generator; the bottom slope was $1/29$. The porous circular pile was constructed with gravel with $d_{50} = 35.5$ mm, a diameter of 3 m, $D_s = 0.1$ m, and $n_0 = 0.419$; it is located at the center of the test area, which has a water depth varying from 0.175 m to 0.275 m.

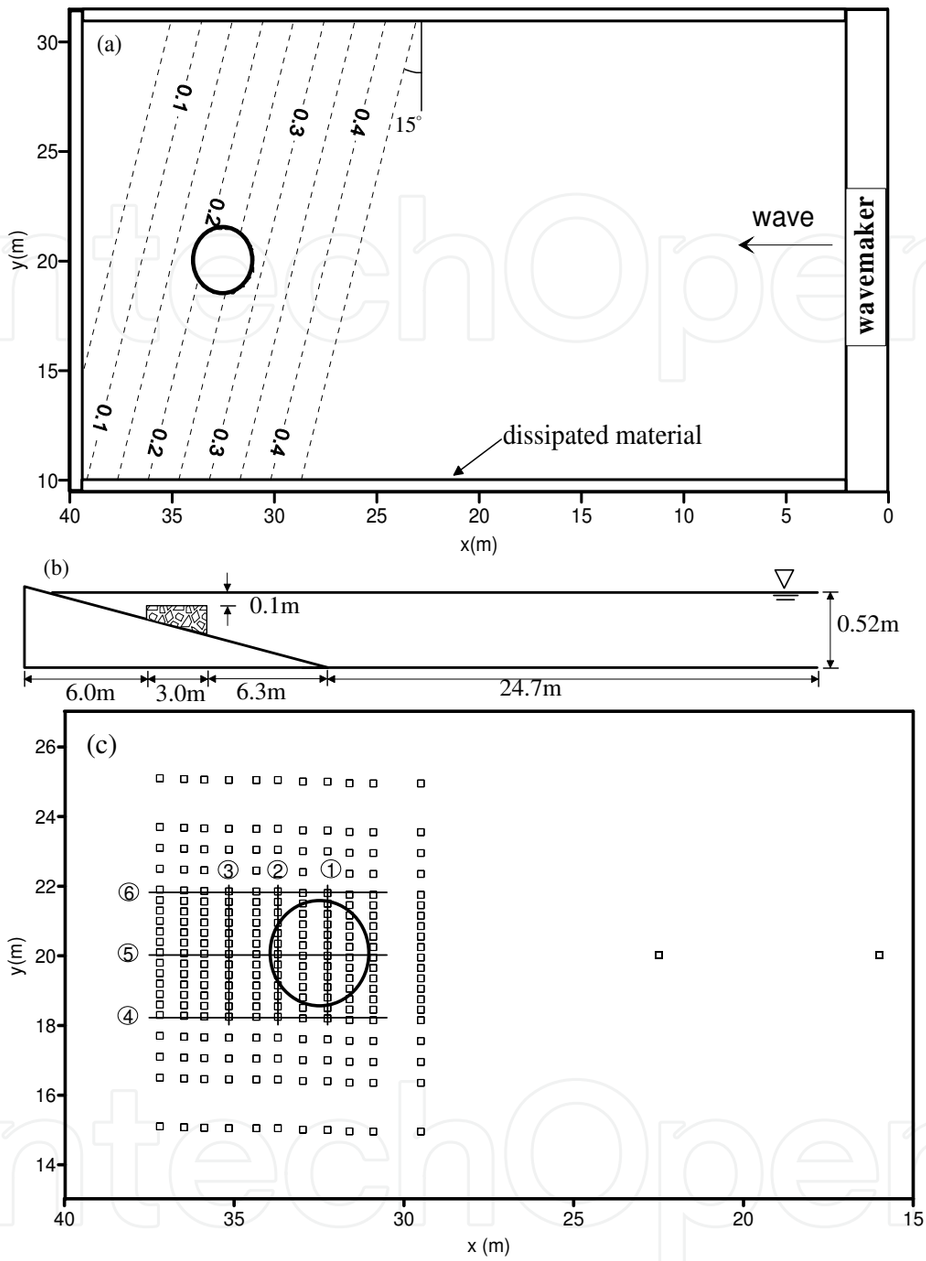

Fig. 6. Laboratory experiment in a wave basin with a submerged permeable circular pile placed on a sloping bottom. (a) plane view; (b) section view; and (c) measuring points of wave gauges.

The still water level in the constant-depth region was maintained at 0.52 m for all experiments. The free surface elevation was measured by 233 capacity-type wave gauges installed at different locations (Fig. 6). The values of intrinsic permeability and turbulent drag coefficient for the circular pile were obtained from water-head experiments, and the results were $k_p = 1.9 \times 10^{-7}$ m^2 and $C_p = 0.1048$, respectively. The incident wave conditions at deep water depth were $H_0 = 0.04$ m, $T = 0.9$ s with normal incident waves.

The porous submerged circular pile acts as a lens and focuses the incoming wave energy into a strong convergence zone. This experiment provides a comprehensive data set that can be used to verify the capability of Hsu et al.'s (2008a) model to predict accurate wave transformation including refraction, diffraction, and energy dissipation due to porous structures on a plane beach. Wave height data were analyzed and collected at many locations within the test zone, along 21 transections (see Fig. 6). The simulated wave heights were compared with the observed data at six selected sections.

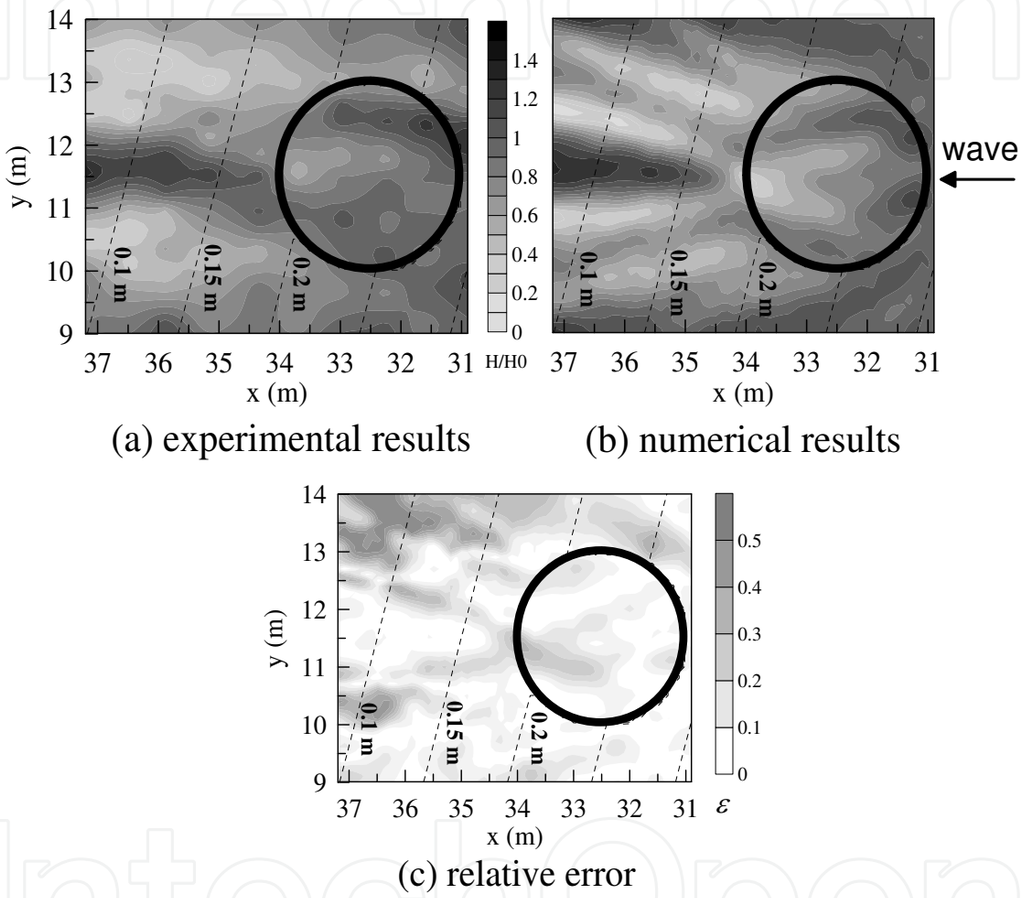

Fig. 7. A comparison of wave patterns around a submerged permeable cylinder. H_0 = 0.04 m, T = 0.9 s. (a) experimental results; (b) numerical results; and (c) relative error $\varepsilon = \left|\left(H_m - H_c\right)/H_m\right|$ between the experimental and numerical results.

Fig. 7(a) and Fig. 7(b) shows the results of relative wave heights of experimental data and numerical data in a planar wave pattern. The comparison between experimental data and numerical data demonstrates that the model is capable of describing the combined effect of wave refraction, diffraction, and porosity. Note that the model predicts a favorable focusing wave pattern. The difference between the numerical calculations and experiments as shown in Fig. 7(c) may be caused by wave reflection from the side walls in the wave basin. Fig. 8 presents comparisons of the wave height variations for all six profiles; it is interesting to note that the numerical results are in good agreement with the experimental observations.

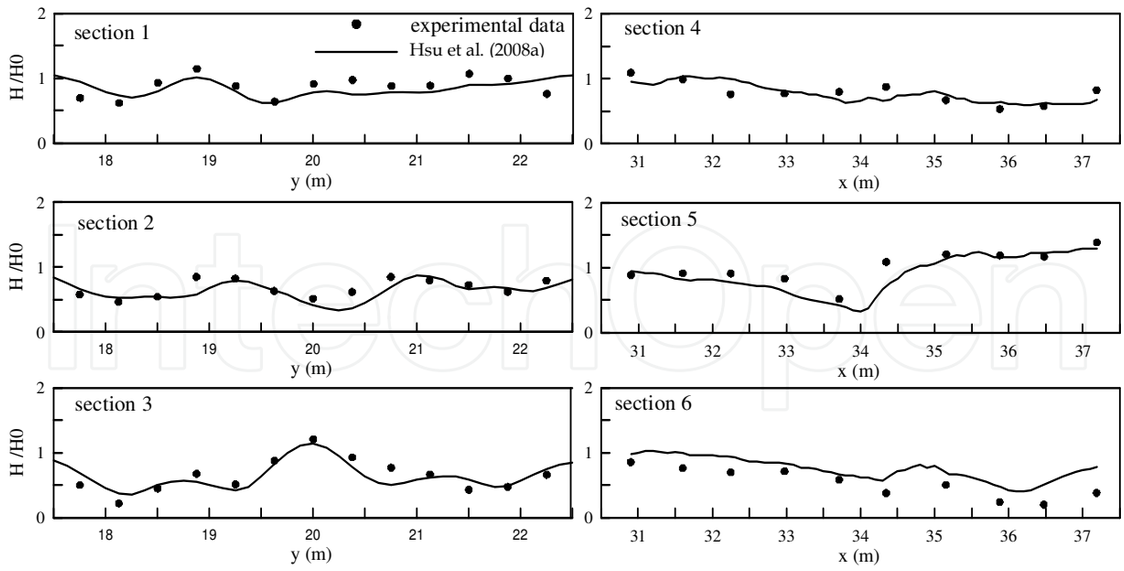

Fig. 8. Comparisons of wave heights at different transactions for waves passing over a submerged circular pile.

5. Model applications

In addition to the laboratory verification, the proposed by Hsu et al.'s (2008a) model was also verified using two typical real cases. The first case simulates wave transformation over a porous elliptical shoal superimposed on a plane beach. The second case tested waves propagating over a permeable submerged breakwater using field data obtained during a field experiment at the CERC Field Research Facility (FRF) in Duck, North Carolina, U.S.A.

In coastal engineering, a porous shoal is generally constructed with gravel or stones for ecological recovery and coastal protection at offshore regions. In the numerical run, the shoal was placed on a sloping bottom with a slope of 1:20, which was rotated clockwise at an angle of 20° from a straight wave paddle and had major and minor radii of 4.0 m and 3.0 m, respectively. The experiment for an impermeable elliptical shoal was conducted by Berkhoff et al. (1982) in a wave basin where the deep mean water depth was h=0.45 m and the incident wave height and period were H_0 = 0.0464 m and T = 1s, respectively. Since the water depth near the wave board was constant, the wave crests generated by the wave paddle traveled in uniform wave trains. According to Eqs. (17) and (18), the typical key parameters of k_p and C_p used in the numerical computation for the porous shoal constructed with gravel of d_{50} = 50 mm and n_0 = 0.20, n_0= 0.39 are summarized in Table 3. For the parabolic MSE model, wave rays and wave height contours for both impermeable (n_0= 0) and permeable shoals (n_0 = 0.20, n_0= 0.39) are shown in Fig. 8. Based on Eqs. (17) and (18), it is noted that different values of the porosity n_0 and different gravel sizes (d_{50} = 50 mm) could yield different values for k_p, C_p, and f_p in the calculation, as listed in Table 3. The numerical result indicates that the wave height continues to increase behind the shoal and decay as the waves reach to the shoreline. The focus of wave trajectories (caustics) is clearer for the impermeable shoal due to the focal phenomenon of wave refraction-diffraction. The comparison in Fig. 9 implies that the combined wave refraction-diffraction effects are rapidly reduced to some extent by the porous structures. A higher porosity of a shoal with a constant grain, gravel or stone diameter would produce a higher attenuation of transmitted waves.

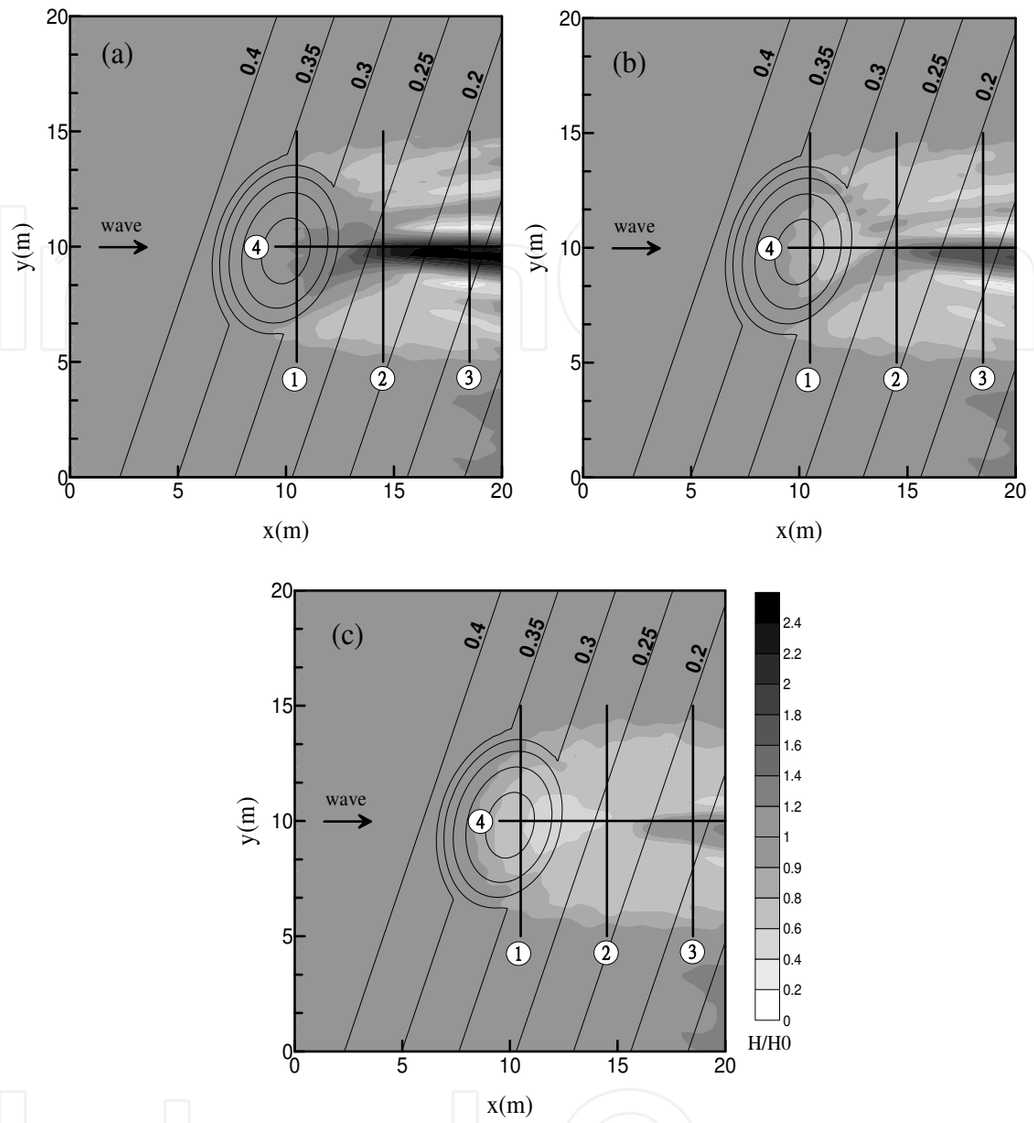

Fig. 9. Calculated wave fields for (a) impermeable ($n_0 = 0.0$), (b) permeable ($n_0 = 0.20$, $d_{50} = 50$ mm), and (c) permeable ($n_0 = 0.39$, $d_{50} = 50$ mm) elliptical shoal on a sloping bottom. The thin solid lines indicate bathymetric contours. The bold solid lines labeled with numbers are transections 1~4 of the wave height distribution, provided for the purpose of comparison. (Hsu et al., 2008a)

When verifying the proposed by Hsu et al.'s (2008a) model, the wave heights are compared at four selected sections, labeled as transections 1~4. A comparison of the computational results with the observations is shown in Fig. 10. It is observed from all the figures that the present model results are in much closer agreement with the experimental data than those of the linear model (Dalrymple et al., 1989) for an impermeable shoal. For any case that involves wave refraction, diffraction, and energy dissipation, it is evident that the present model is capable of accomplishing this job. Notably, Fig. 10 shows that the focus is clearly reduced by the porosity of the shoal.

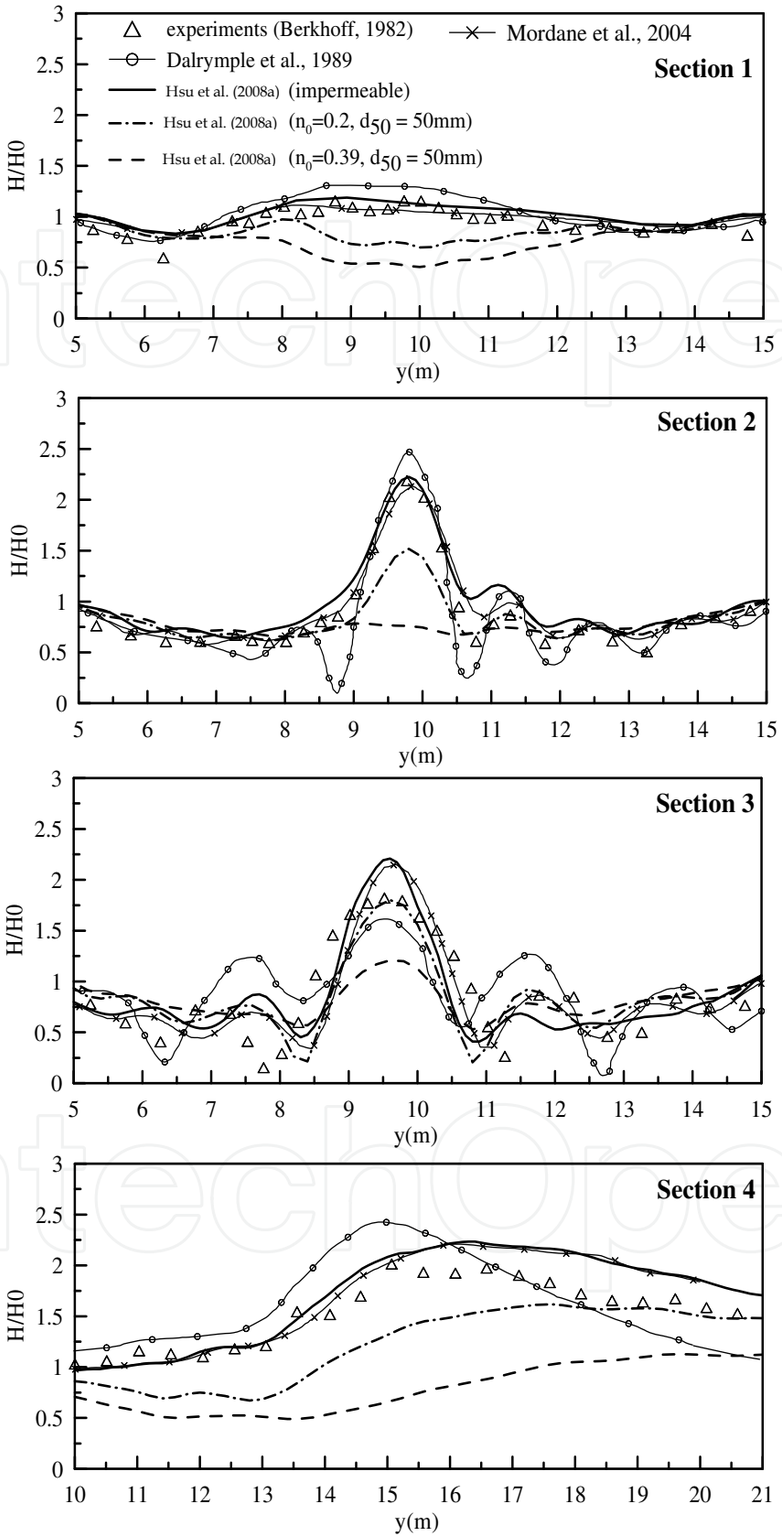

Fig. 10. Comparison of the model results (n_0 = 0, 0.2, 0.39) against experimental data by Berkhoff et al. (1982) along sections 1~4, respectively (see Fig. 9).

n_0	d_{50} (mm)	k_p (m^2)	C_p	f_p
0.20	50	2.6E-8	0.06	0.372
0.39	50	6.0E-7	0.15	0.565

Table 3. Key parameters used in the computation of elliptical shoal

The bathymetry in the FRF coastal area is generally straight and parallel to the coastline, except in the vicinity of the research pier, as shown in Fig. 11. The pier was built in order to collect field data. Two cases with and without a submerged breakwater were designed for simulating a wave field using the available wave data in the numerical calculation. The submerged breakwater hass a length, width, and length of 200 m, 30 m, and 2.5 m, respectively, and it comprised large stones; it was placed at a water depth of $h = 4$ m. For a practical engineering design, the porosity and stone size of the submerged breakwater were taken as $n_0 = 0.49$ and $d_{50} =$ 1,000 mm. The values of $k_p = 1.025 \times 10^{-4}$ m^2 and $C_p = 0.173$ were then obtained from Eqs. (17) and (18). The input monochromatic wave conditions are $H_0 = 1.56$ m, $T = 6.87$ s, and $\theta_0 = 43^\circ$, based on field observations.

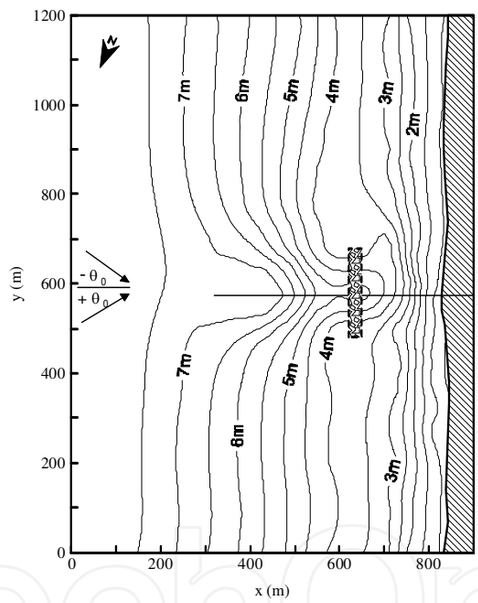

Fig. 11. Application of model for a complicated bathymetry constructed using a permeable submerged breakwater in the FRF pier, Duck, North Carolina, U.S.A.

From Fig. 12(a), we notice that the scouring hole causes the wave energy to diverge, inducing a reduction in the wave height along the pier without a structure. For the construction of the submerged breakwater, Fig. 12(b) demonstrates that the model reproduces the general wave height variation due to wave refraction, diffraction, wave breaking, and energy dissipation. Comparisons between the model results and observed data for field verification without a structure are presented in Fig. 13. The results show that the proposed model accurately predicts wave propagation for these types of wave conditions over a complicated bathymetry. It is also noted that the model does decay the wave height on account of refraction, diffraction, wave breaking, and porosity behind the submerged detached breakwater.

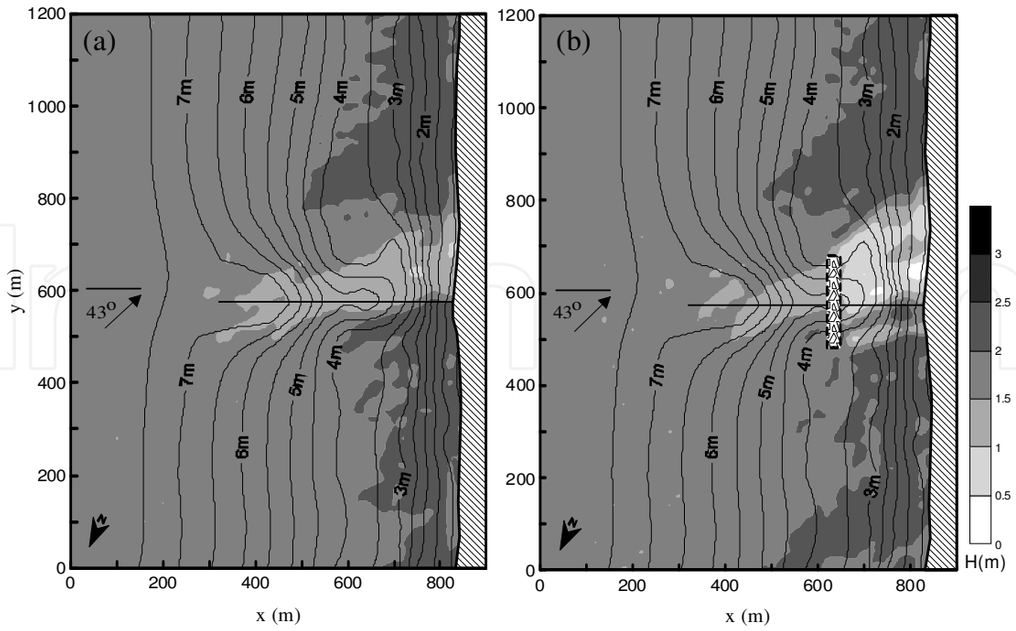

Fig. 12. Planar wave patterns (a) with and (b) without a permeable submerged breakwater on a complicated bathymetry at FRF coastal area, Duck, North Carolina, U.S.A. The line at the center represents the FRF pier.

6. Evolution Equation of Mild-Slope Equation (EEMSE)

To further consider the effect of wave reflection, the EEMSE was developed by Hsu et al. (2008b) to simulate waves propagation over a porous structure. Following Hsu et al. (2008b) a numerical model which includes wave-porous media interaction, wave reflection, wave breaking and dissipation was presented. Eq.(10) can be expressed as

$$-\left[\left(2i\omega\right)/\alpha_p\right]\varphi_t = \nabla_h{}^2\varphi + k_c^2\varphi \tag{28}$$

The radiation boundary condition (RBC) in the model is specified so that waves are forced to go out radically along the bounder of a computational domain. There are two types of RBC: a full or partial reflection radiation boundary condition and a given boundary condition which are specified along the boundary of x and y directions as follows, respectively.

$$\phi_x = \pm\left(-1\right)^m i\alpha\phi k\cos\theta + 2i\phi_i k\cos\theta \tag{29}$$

$$\phi_y = \pm\left(-1\right)^m i\alpha\phi k\sin\theta \tag{30}$$

where $\alpha = (1-R)/(1+R)$ is an absorption coefficient; R is a reflection coefficient, θ is the approaching wave angle to the boundary; and ϕ_i denotes a given velocity potential at the boundary of incident waves. For full reflection, $\phi_i = 0$, $m = 0$, and $\alpha = 0$; for partial reflection, $\phi_i = 0$, $m = 0$, and $0 < \alpha \le 1$; and for a given boundary condition, $m = 1$ and $\alpha = 1$. For this case, the velocity potential is assumed in the form

$$\phi = A(x,y)e^{i(kx\cos\theta + ky\sin\theta - \omega t)} \tag{31}$$

where $A(x,y)$ is the amplitude of the velocity potential. From Eq. (31), we have

$$\frac{1}{k^2}\frac{\partial^2\phi}{\partial^2 y} = \phi\sin^2\theta \tag{32}$$

For full transmitted waves along the boundary, Eq. (30) is reduced to Eq.(15). In this model wave diffraction, refraction, reflection and breaking from porous structures were considered.
The model is validated for wave propagating over a single cylindrical impermeable pile rest on a protecting cylindrical impermeable or permeable step. A typical case was performed by Hsu et al., (2009). Fig. 13 presents the bathymetry of a single cylindrical pile rest on a protecting cylindrical step. The impermeable cylinder has a radius of $r_a = L/4$ and the radius of the cylindrical protection is $r_b = L/2$, where L is the wavelength. The wave incidence is equal to 45°. The incident wave height is $H_0 = 0.03$ m. The results of analytical solutions presented by Silva et al. (2003) and predicted dimensionless wave amplitude fields are shown in Fig. 14. Fig. 15 shows the result of wave propagation over a single cylindrical impermeable pile on a protecting cylindrical permeable step ($n_0 = 0.4$, $f_p = 1.0$).

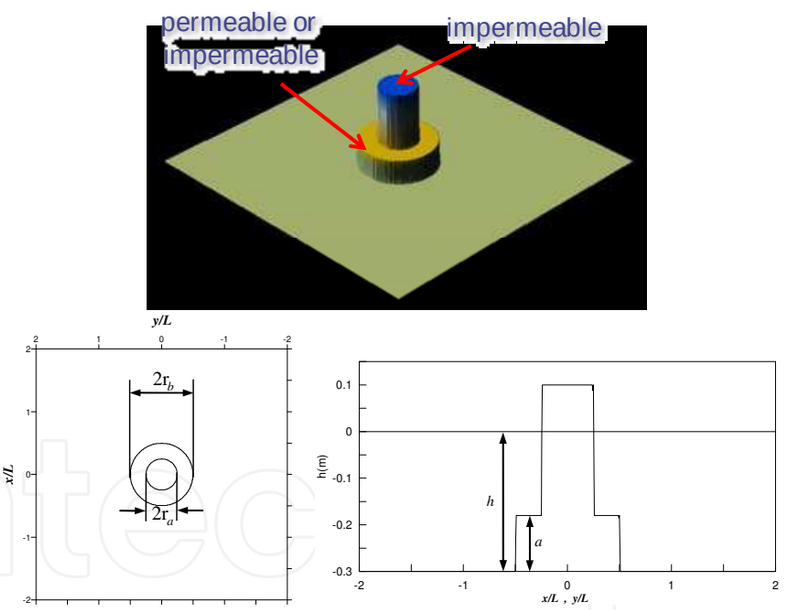

Fig. 13. Bathymetry of a single cylindrical pile on a protecting cylindrical step

In this two figures, the compared profile is along the x/L= 0 and y/L= 0 axes. Comparing with theoretical results and present model, it is clear that the numerical prediction is in good agreement with the analytical solution.
The model is also applied to simulate wave transformation on a group of five vertical porous cylinders. Each cylinder has a radius = L/4. In Fig. 16, the four cylinders are located at the vertices of a square of side dimension which is equal to 2L and the fifth one is located at the centre. The incident wave condition is the same with Fig.15. Fig. 17 shows the wave pattern for waves propagating over a group of five vertical permeable cylinders. The results

of analytical and numerical dimensionless wave amplitude fields are compared with in Fig. 17 and good agreement is found.

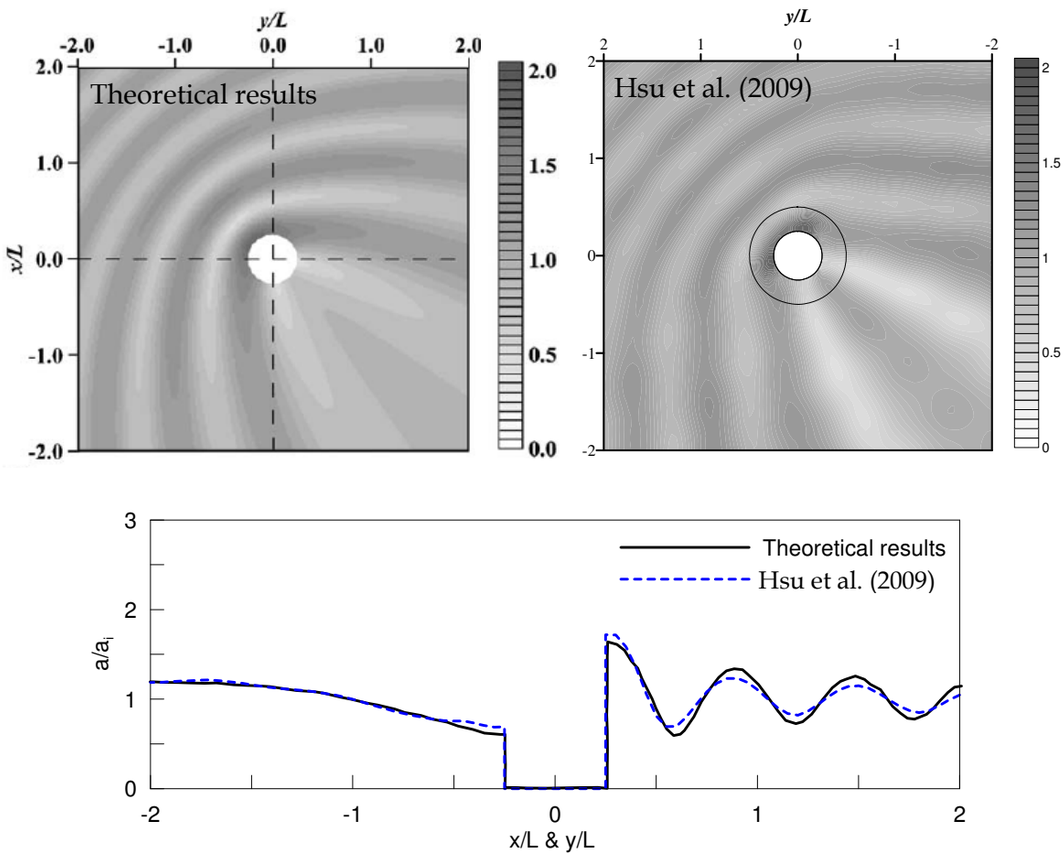

Fig. 14. Wave propagation over a single cylindrical impermeable pile on a protecting cylindrical impermeable step ($n_0 = 0$, $f_p = 0$)

7. Conclusions

A numerical wave model has been developed by Hsu et al. (2008a; 2008b; 2009) for wave propagation over porous structures on the basis of an evolution equation of mild-slope equation (EEMSE), including wave breaking and energy dissipation. The model is simple and it incurs a lower computational cost even when modeling large coastal areas. For progressive waves, the validity of the present model is verified through comparisons with the experimental data and analytical solutions for waves propagating over porous structures. The model is further applied to the practical cases of a permeable elliptical shoal and a submerged permeable breakwater on a complicated bathymetry. Since a higher-order quadratic rational function of the Padé [2,2] approximation is employed in the finite difference discretization, the accuracy of model prediction can be improved.

The wave reflection is also considered in the present parabolic approximation. The MSE developed for describing wave transformation over porous structures is initially well suited

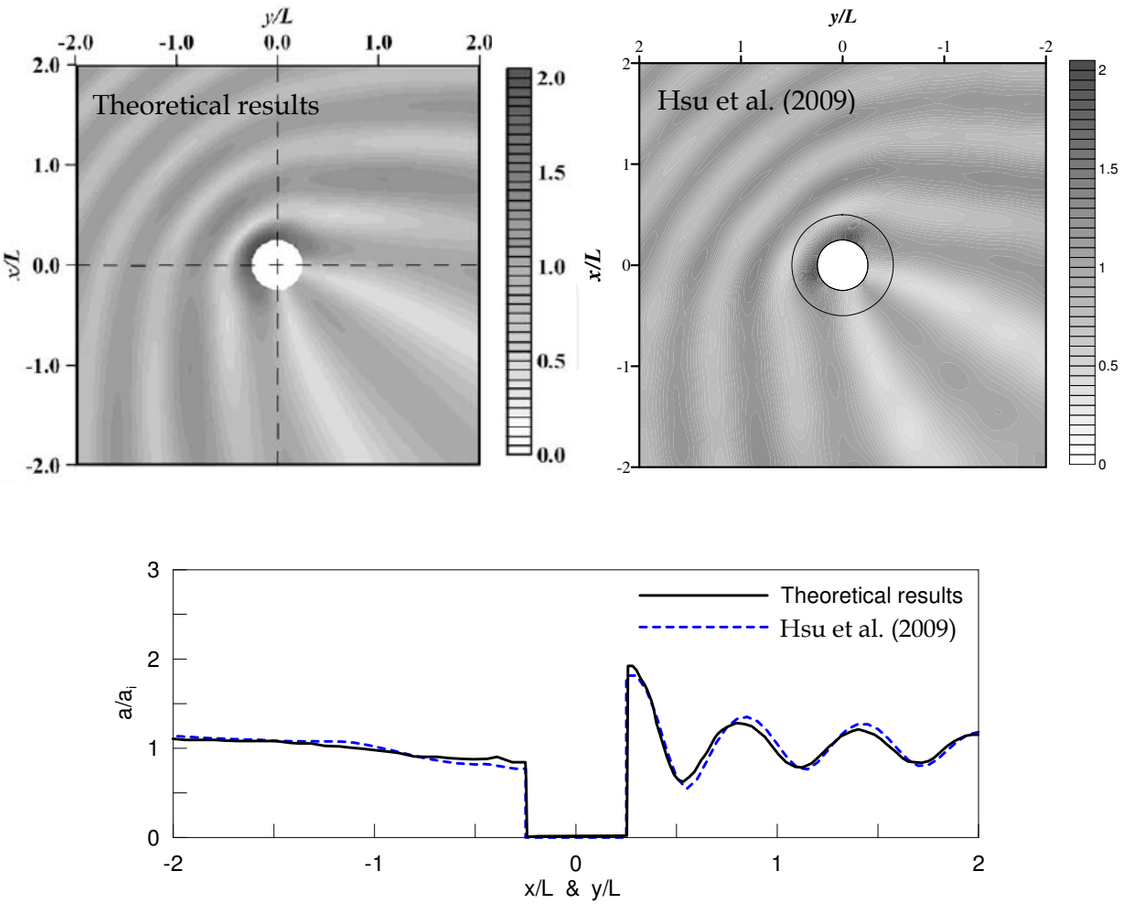

Fig. 15. Wave propagation over a single cylindrical impermeable pile on a protecting cylindrical permeable step ($n_0 = 0.4$, $f_p = 1.0$)

for examining wave interaction with submerged structures. In some cases, reflection might be important for submerged porous structures or waves traveling on a steep sloping beach. However, the combined effect of wave refraction and diffraction for simulating coastal processes is the focus of the parabolic model. For this reason, the parabolic MSE of Mordane et al. (2004) is extended to account for wave propagation over submerged permeable structures. A further development of the parabolic MSE for porous structures including reflection is also carried out by Hsu et al. (2008b).

The other restriction of the parabolic MSE is that it is applicable only to regular waves. In real situations, the sea state is random; therefore, it would be more realistic if the present model could be used to describe wave transformation of porous structures for irregular waves. Following Panchang et al. (1990) and Suh et al. (1997), the present MSE can be modified to derive a wave spectral calculation.

Furthermore, the model can be applied to submerged structures with multiple permeable layers. The concept of equivalent work may be utilized to set a monoporous layer to represent a single layer. The validity of this approach should be examined through experimental data.

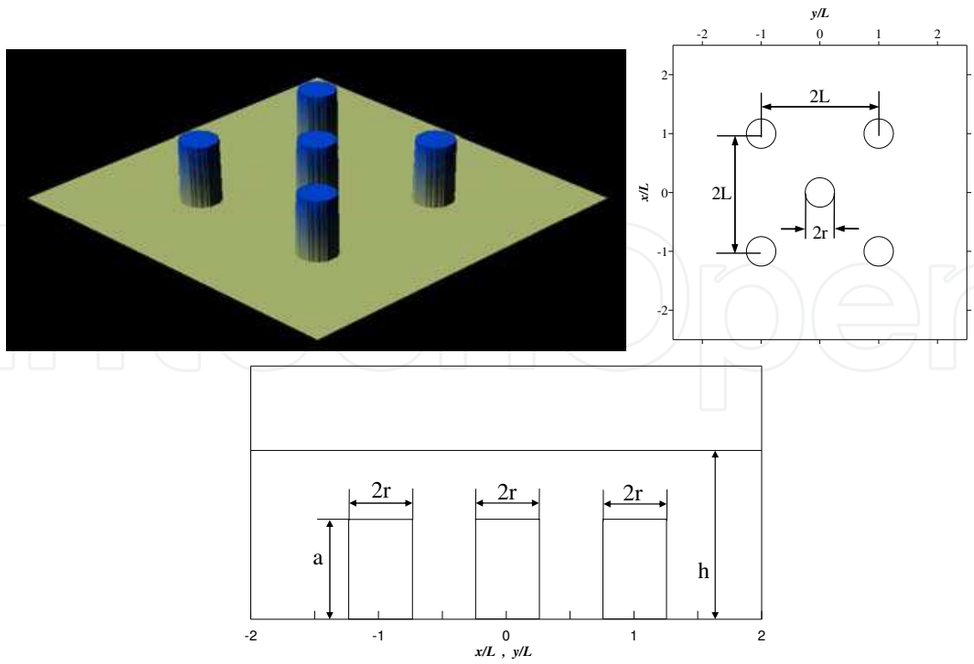

Fig. 16. Bathymetry of a group of five vertical cylinders

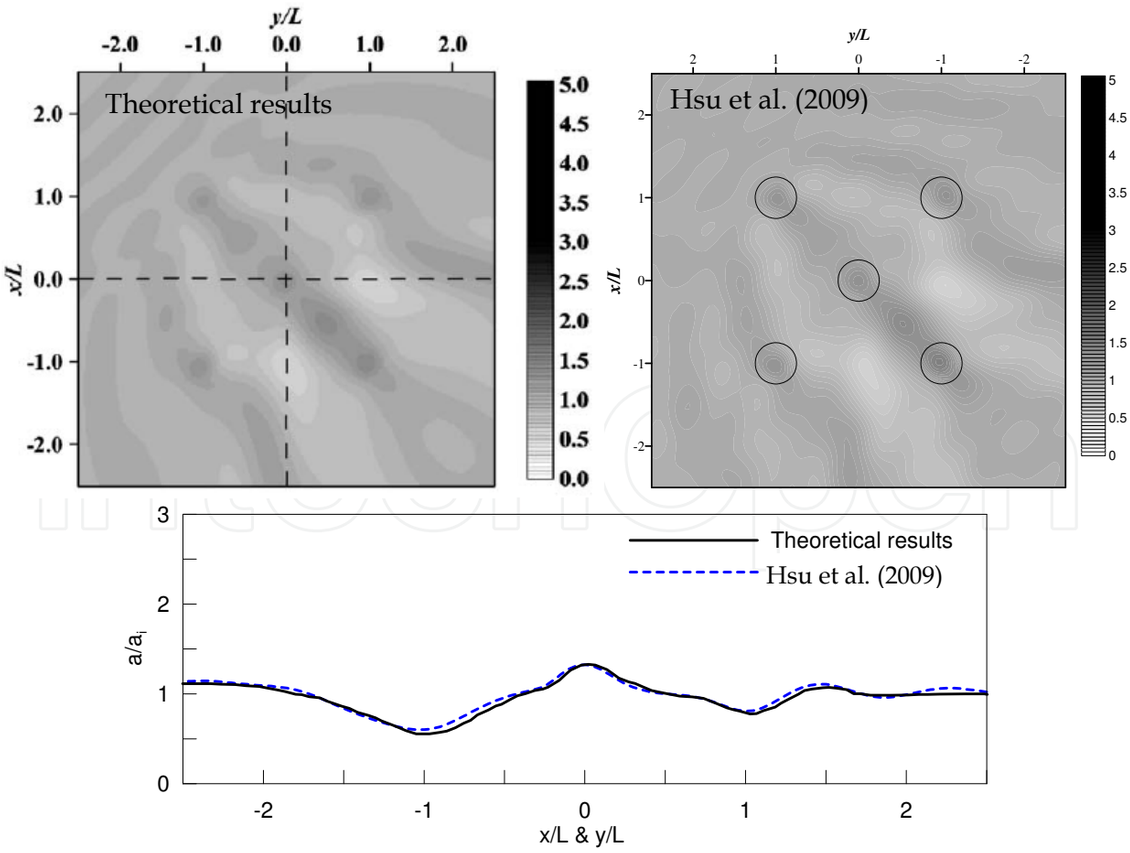

Fig. 17. Wave propagation over a group of five vertical permeable cylinders (n_0 = 0.4, f_p = 1.0)

8. References

Arbhabhiramar, A.M., Dinoy, A.A. (1973). Friction factor and Reynolds number in porous media flow. *Journal of Hydraulic Division 99 (HY6)*, pp. 901-911

Battjes, J.A., Janssen, J. P. F. M. (1978). Energy loss and set-up due to breaking in random waves. *Proceedings of 16th International Conference on Coastal Engineering*, Hamburg, pp. 569-578.

Berkhoff, J.C.W., Booij, N., Radder, A.C. (1982). Verification of numerical wave propagation models for simple harmonic linear water waves. *Coastal Engineering 6*, pp.255- 279.

Cruz, E.C., Isobe, M., Watanabe, A. (1997). Boussinesq equation for wave transformation on porous beds. *Coastal Engineering 30*, pp.125- 156.

Dally, W.R., Dean, R.G., Dalrymple, R.A. (1985). Wave height variation across beaches of arbitrary profile. *Journal of Geophysical Research 90 (C6)*, pp.11917-11927.

Dalrymple, R.A., Suh, K.D., Kirby, J.T., Chae, J.W., 1989. Models for very wide-angle water waves and wave diffraction. Part 2 : Irregular bathymetry. *Journal of Fluid Mechanics 201*,pp. 299-322.

Ebersole, B.A., Cialone, M.A., Prater, M.D. (1986). Regional coastal processes numerical modeling system. Report 1: RCPWAVE, Department of the Army, Waterway Experiment Station, Corps of Engineers.

Furukawa, K., McDougal, W.G. (1991). Wave diffraction due to trenches and rubble. Report No. 166, Department of Civil Engineering Report, Oregon State University, Corvallis, OR.

Goda, Y. (1970). A synthesis of breaker indices. *Proceedings of 17th International Conference on Coastal Engineering, Vancouver*, Sydney , pp. 471- 490.

Hsu, T.W. and Wen, C.C., (2001). A parabolic equation extended to account for rapidly verying topography. *Ocean Engineering* 28, pp.1479-1498.

Hsu, T.W., Chang, J.Y., Lan, Y.J. and Ou S.H. (2008a). A parabolic equation for wave propagation over porous structures. *Coastal Engineering* 55, pp. 1148-1158.

Hsu T.W., Chang, J.Y., Lin, T.Y. (2008b). An Evolution Equation of Mild-Slope Equation for Water Waves Propagation over Porous Media with Large Angle Incidence. *Proceedings of 31th International Conference on Coastal Engineering, Hamburg, Germany*.

Hsu, T.W., Chang, J.Y., Lan,Y.J. (2009). Modeling of water waves over submerged permeable structures with larger angle. A paper submitted to Coastal Engineering.

Isobe, M. (1987). A parabolic equation model for transformation of irregular waves due to refraction, diffraction and breaking. *Coastal Engineering in Japan* 30, pp.33-47.

Kirby, J.T., Dalrymple, R.A. (1991). User's manual, combined refraction/diffraction model. Center for Applied Coastal Research, Department of Civil Engineering, University of Delaware, Newark, De19716, REF/DIF 1, 2.3.

Lara, J.L., Losada, I.J., Liu, P.L.F. (2006). Breaking waves over a mild gravel slope: Experimental and numerical analysis. *Journal of Geophysical Research* 111, C11019.

Losada, I.J., Silva, R., Losada, M.A. (1996). Interaction of non–breaking directional random waves with submerged breakwaters. *Coastal Engineering* 28, 249-266.

Losada, I.J., Patterson, M.D., Losada, M.A. (1997). Harmonic generation past a submerged porous step. *Coastal Engineering* 31, 281-304.

Madsen, O.S. (1974). Wave transmission through porous structure. *Journal of Waterway, Port, Coastal, and Ocean Engineering* 100, 169-188.

Mèndez, F.J., Losada, I.J, Losada, M.A. (2001). Mean magnitudes induced by regular waves in permeable submerged breakwaters. *Journal of Waterway, Port, Coastal, and Ocean Engineering* 127(1), 7-15.

Miche, R. (1951). Le povoir réfléchissant des ouvrages maritime exposés à l'action de la houle, *Annales Ponts et Chausseess*, 121 Annee, 285-319.

Mordane, S., Mangoub, G., Maroihi, K.L., Chagdali, M. (2004). A parabolic equation based on a rational quadratic approximation for surface gravity wave propagation. *Coastal Engineering* 50, 85-95.

Nagayama, S. (1983) Study on the change of wave height and energy in the surf zone. Bachelor Thesis, Yokohama National University, 80p, Japan.

Panchang, V.G., Ge, W., Pearce, B.G., Briggs, M.J. (1990). Numerical simulation of irregular wave propagation over shoal. *Journal of Waterway, Port, Coastal, and Ocean Engineering* 116(3), 324-340.

Radder, A.C. (1979). On the parabolic equation method for water wave propagation. Journal of Fluid Mechanics 95, 159-176.

Rojanakamthorn, S., Isobe M., Watanabe A. (1989). A mathmatical model of wave transformation over a submerged breakwater. *Coastal Engineering in Japan* 32 (2), 209-234.

Rojanakamthorn, S., Isobe, M., Watanabe, A. (1990). Modeling of wave transformation on submerged breakwater. *Proceedings of 22th International Conference on Coastal Engineering*, Delft, The Netherlands, pp. 1060-1073.

Silva, R., Losada, M.A., Salles, P. (2006) Modelling linear wave transformation induced by dissipative structures—Regular waves. Ocean Engineering 33, pp.2174–2194

Sollitt, C.K., Cross, R.H. (1972). Wave transmission through permeable breakwaters. *Proceedings of 13th International Conference on Coastal Engineering*, Vancouver, pp. 1827-1846.

St. Mary, D.F. (1985). Analysis of an implicit finite difference scheme for very wide angle underwater acoustic propagation. *Proceedings of 11th IMACS World Congress on System Simulation and Scientific Computation*, Oslo, pp. 153-156.

Suh, K.D., Lee, C., Park, W.S. (1997). Generation of waves in Boussinesq models using a source function method, *Coastal Engineering* 32, 91-117.

Watanabe, A., Dibajnia M. (1988). A numerical model of wave deformation in surf zone. *Proceedings of 21th International Conference on Coastal Engineering*, Malaga, Spain, pp. 578-587.

Wave Propagation in Materials for Modern Applications

Edited by Andrey Petrin

ISBN 978-953-7619-65-7
Hard cover, 526 pages
Publisher InTech
Published online 01, January, 2010
Published in print edition January, 2010

In the recent decades, there has been a growing interest in micro- and nanotechnology. The advances in nanotechnology give rise to new applications and new types of materials with unique electromagnetic and mechanical properties. This book is devoted to the modern methods in electrodynamics and acoustics, which have been developed to describe wave propagation in these modern materials and nanodevices. The book consists of original works of leading scientists in the field of wave propagation who produced new theoretical and experimental methods in the research field and obtained new and important results. The first part of the book consists of chapters with general mathematical methods and approaches to the problem of wave propagation. A special attention is attracted to the advanced numerical methods fruitfully applied in the field of wave propagation. The second part of the book is devoted to the problems of wave propagation in newly developed metamaterials, micro- and nanostructures and porous media. In this part the interested reader will find important and fundamental results on electromagnetic wave propagation in media with negative refraction index and electromagnetic imaging in devices based on the materials. The third part of the book is devoted to the problems of wave propagation in elastic and piezoelectric media. In the fourth part, the works on the problems of wave propagation in plasma are collected. The fifth, sixth and seventh parts are devoted to the problems of wave propagation in media with chemical reactions, in nonlinear and disperse media, respectively. And finally, in the eighth part of the book some experimental methods in wave propagations are considered. It is necessary to emphasize that this book is not a textbook. It is important that the results combined in it are taken “from the desks of researchers“. Therefore, I am sure that in this book the interested and actively working readers (scientists, engineers and students) will find many interesting results and new ideas.

Slavka Krautzeka 83/A
51000 Rijeka, Croatia
Phone: +385 (51) 770 447
Fax: +385 (51) 686 166
www.intechopen.com

No.65, Yan An Road (West), Shanghai, 200040, China
中国上海市延安西路65号上海国际贵都大饭店办公楼405单元
Phone: +86-21-62489820
Fax: +86-21-62489821

IntechOpen

IntechOpen